Review of Scientific Instruments ARTICLE pubs.aip.org/aip/rsi

Electromagnetic pulse protective shielding for digital x-ray detectors

Cite as: Rev. Sci. Instrum. 94, 075106 (2023); doi: 10.1063/5.0160120
Submitted: 30 May 2023 • Accepted: 4 July 2023 •
Published Online: 21 July 2023 • Publisher Error Corrected: 28 July 2023

Stephan Schreiner,[1,a)] Constantin Rauch,[1] Bernhard Akstaller,[1] Paulina Bleuel,[1] Eric Fröjdh,[2] Artem S. Martynenko,[3] Aldo Mozzanica,[2] Paul Neumayer,[3] Leonard Wegert,[3] Bernhard Zielbauer,[3] Adrian Zink,[1] Gisela Anton,[1] Thilo Michel,[1] and Stefan Funk[1]

AFFILIATIONS

[1] Erlangen Centre for Astroparticle Physics (Ecap), Friedrich-Alexander Universität Erlangen-Nürnberg, Nikolaus-Fiebiger-Straße 2, 91058 Erlangen, Germany
[2] Paul Scherrer Institut (Psi), Forschungsstrasse 111, 5232 Villigen, Switzerland
[3] Gsi Helmholtzzentrum für Schwerionenforschung GmbH, Planckstraße 1, 64291 Darmstadt, Germany

[a)] **Author to whom correspondence should be addressed:** Ste.Schreiner@fau.de

ABSTRACT

Laser-driven x-ray backlighting can be used to image fast dynamic processes like the propagation of laser-driven shock waves in matter. We demonstrate and evaluate the feasibility of operating the JUNGFRAU detector designed by PSI, a direct detecting x-ray detector, in environments with extreme electromagnetic pulses. The electromagnetic pulse-protective housing is specifically designed for this detector and optimized for pump-probe experiments at the Petawatt High-Energy Laser for Heavy Ion EXperiments (PHELIX) facility at the GSI Helmholtzzentrum für Schwerionenforschung GmbH. The beryllium x-ray entrance window of the protective housing has a high x-ray transmission of 94% at 8 keV. Measurements have shown that the housing simultaneously provides a relative damping of the electromagnetic field on average higher than 1000 in the frequency range of 100 MHz to 5 GHz. The results demonstrate the feasibility of operating digital detectors in experiments where strong electromagnetic pulses are present.

I. INTRODUCTION

X-ray imaging is an indispensable diagnostic technique in high-energy density science and laboratory astrophysics experiments. In inertial confinement fusion, x-ray radiography is routinely used to access implosion uniformity and the imploding shell's velocity.[1] In laboratory astrophysics experiments, radiography has been the main diagnostic for imaging the interaction of high mach-number flows with dense obstacles[2,3] or for observing interface instabilities from a blast wave traversing an interface comparable to models of type-II supernova explosions.[4]

These pump-probe experiments are commonly performed at high-power laser facilities like, e.g., LULI2000, PHELIX, or ELI Beamlines. A laser-beam irradiates a small target, depositing energy in the target, launching strong shock waves, and thereby initiating hydrodynamic events. The event is probed by x-ray imaging. The x-rays are generated with a backlighter, a small solid target irradiated with a second laser pulse. The laser plasma generated in the backlighter material emits a broad x-ray spectrum.[5] Beside this high-energetic electromagnetic radiation, up to 0.1% of the laser energy is released in the GHz and THz regimes[6] as electromagnetic pulses (EMP).

Electromagnetic pulses disturb digital devices in the experiment area.[6] For imaging, one solution to this problem has been the use of analog imaging plates (IPs). However, this approach has significant drawbacks. First and foremost, the image quality of IPs is typically worse than that of modern (high-quality) digital x-ray detectors. Furthermore, IPs require readout. If placed inside the vacuum chamber, venting and reevacuating are needed, limiting the repetition rate of experiments. Modern laser facilities like the ELI Beamlines in Prague aim for a 10 Hz repetition rate, making it impossible to use analog IPs.[6]

For stable operation of digital devices in this harsh environment, EMP-generation is investigated and mitigation strategies are

developed.[6] Dedicated housings for digital devices can be designed to shield the device from the EMP. Consoli *et al.*[6] presented an overview of existing solutions and construction guidelines. However, to our knowledge, there is no suitable ready-to-use case or design suggestion for an EMP-proof housing for digital x-ray detectors. The challenge is to keep GHz and THz radiation out while being transparent for tender and hard x-rays. Kocon *et al.*[7] demonstrated the operation of a battery powered Timepix detector enclosed in a 1.5 mm thick fully welded copper box. Copper of 1.5 mm and aluminum of 30 μm were tested as an EMP-safe x-ray entrance window and showed enough protection to operate the detector. Data input–output and triggering were realized with a fiber-only connection. Although this concept works for smaller detectors with low power consumption, it is not feasible for more sophisticated detectors with higher power consumption and active cooling. Furthermore, the vacuum window and the 30 μm of aluminum absorb considerable amounts of photons in the keV energy range.

II. THE DIGITAL X-RAY DETECTOR AND ITS EMP PROTECTION

For digital detectors that require a significant amount of infrastructure, we present a novel EMP-proof housing. Our x-ray detection system is highly sensitive in the energy range from 10 to 13 keV in order to exactly fit the requirements of an experiment conducted at the PHELIX laser facility (detailed explanation of this experiment in Sec. III). Hence, the EMP shielding of the detector must provide a highly transmissive entry window for x rays in this energy regime. With a transmission of 94% at 8 keV photon energy, 300 μm thick high-purity beryllium windows serve this purpose very well. The housing was successfully implemented to protect a JUNGFRAU detector placed in the target chamber of the Petawatt High-Energy Laser for Heavy Ion EXperiments (PHELIX) facility. Additionally, Möbius antennas were used to quantify the EMP protection of the housing in the GHz regime.

A. The digital detector

The detector used during the experiment is the adJUstiNg Gain detector FoR the Aramis User station (JUNGFRAU), initially developed at the Paul Scherrer Institute (PSI) for synchrotron[8] and XFEL-light sources.[9] The silicon-based 320 μm thick sensor has a high absorption of 73% at 12 keV,[10] decreasing fast for higher x-ray energies. The JUNGFRAU detector is capable of framerates up to 2.2 kHz with a resolution of 512 × 1024 pixels and a pixel pitch of 75 μm. It returns, after gain calibrations are applied per pixel, the absorbed energy per x-ray photon in keV units, making it uniquely suited for backlighter experiments, where x-ray source parameters can vary widely between shots.

The detector requires active liquid cooling to keep the sensitive area at constant and low temperatures. Operating the detector with exposure times of 10–50 μs at a sensor temperature of 16 °C is sufficient. However, decreasing the temperature reduces the thermal noise. Hence, during this experiment, the sensor was cooled down below 0 °C. Additionally, the detector requires a power cable, a standard Ethernet cable for detector control, a fiberoptic link for data download, a trigger connection, and a hose for dry nitrogen. These connections need to be passed through the EMP housing to the outer environment without compromising the EMP protection. This poses challenges for the design of the protection.

To our knowledge, the JUNGFRAU detector has never before been successfully operated at a laser-driven x-ray backlighter facility.

B. The EMP-proof box

The basic idea of the protective EMP box is to create a Faraday cage. A half-cut of the computer aided design (CAD) model can be seen in Fig. 1. The x rays enter the box from the right side, propagate through two beryllium windows (2.1) and (2.2), and are detected by the JUNGFRAU detector ③. A photograph of the box can be found in Fig. 2.

The box is made of stainless steel and uses standard vacuum components wherever possible. To guarantee a tight conductive connection between components that are not welded together, aluminum seals were used. This allows us to build the housing in multiple pieces, use it as a vacuum chamber and guarantee a certain amount of flexibility in the experimental setup. The outer protective layer ①, marked by the blue line, features an 80 × 80 mm^2 wide and 300 μm thick beryllium window (2.1), which is electrically conductive and soldered onto a flange. The JUNGFRAU detector ③ is placed in a vacuum-proof housing ④, marked by the green line, which is also constructed as a Faraday cage equipped with a beryllium window of the same size (2.2). The detector is connected to the outside via the flexible hose ⑤. In this hose, the cables are guided to the outside and fed through stainless steel pipes to the computer, which is also placed in its outer Faraday cage. Therefore, the EMP protection consists of a two-stage Faraday cage. As the EMP measurements have shown (see Sec. III C), the damping of the outer Faraday cage would already have been sufficient to protect the x-ray detector.

The EMP box is connected via a standard CF 200 flange ⑥ to the outer wall of the target chamber ⑦. During the experiment, the target chamber is vented about every 90 min. To keep the detector at a constant low temperature without any water condensation occurring, the outer Faraday cage ①, in combination with the vacuum valve ⑧, additionally serves as an independent vacuum chamber. This chamber is pumped with a table-top turbo pump from the ISO-63 flange ⑨ on the rear side. By opening the valve, the small vacuum chamber is connected to the large experimental chamber. Compared to a vacuum window, this has the advantage of not adding another filter to the x-ray beam path.

To avoid pressure differences at the beryllium windows and minimize the danger of them breaking, the volumes behind the windows are ventilated by providing a connection to the other side of the window. This connection is realized with 21 holes with a diameter of d = 2mm drilled into 20 mm stainless steel. To be able to vary this ventilation in future experiments, this array ⑩ is welded to a CF 16 flange. The damping of the ventilation is estimated as follows According to Yoon *et al.*,[11] the cut-off frequency f_C of an electromagnetic wave propagating through a waveguide with a diameter d can be calculated by

$$f_C = \frac{1.8412}{\pi \cdot d} \cdot c_0, \tag{1}$$

with the vacuum velocity of light c_0 and 1.8412 as constant factors for the main mode of the electromagnetic wave. For our setup,

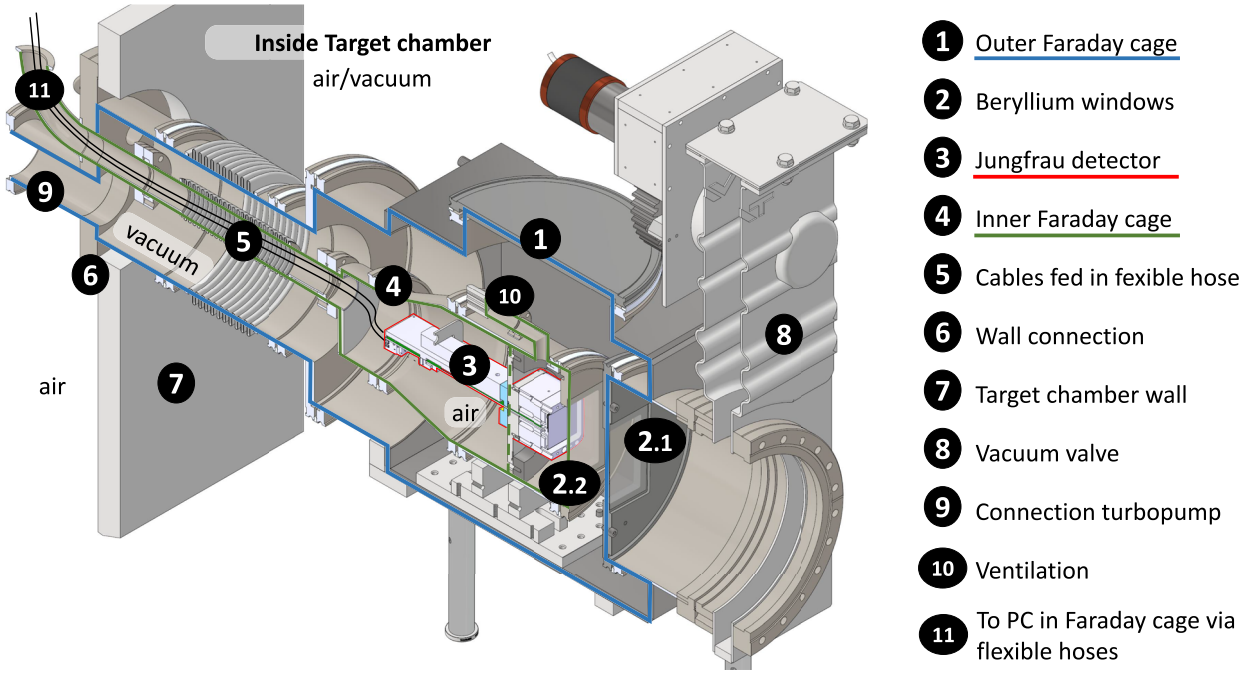

FIG. 1. Half cut of the EMP box developed for the JUNGFRAU detector. The blue line ① marks the outer Faraday cage. In combination with the vacuum valve ⑧, this cage serves as an independent vacuum box that can be joined with the vacuum in the experimental chamber. The housing of the JUNGFRAU detector ④ serves as a second Faraday cage (green line). The barrier between vacuum and air is marked with the dashed green line. The beryllium windows (2.1) and (2.1) assure high x-ray transmission while keeping the conductivity of the housing intact. During the experiment at the PHELIX laser (see Sec. III), the EMP source is positioned about 0.8 m in front of the beryllium window (2.2). An interactive PDF with the CAD model can be found in the supplementary material, Sec. V.

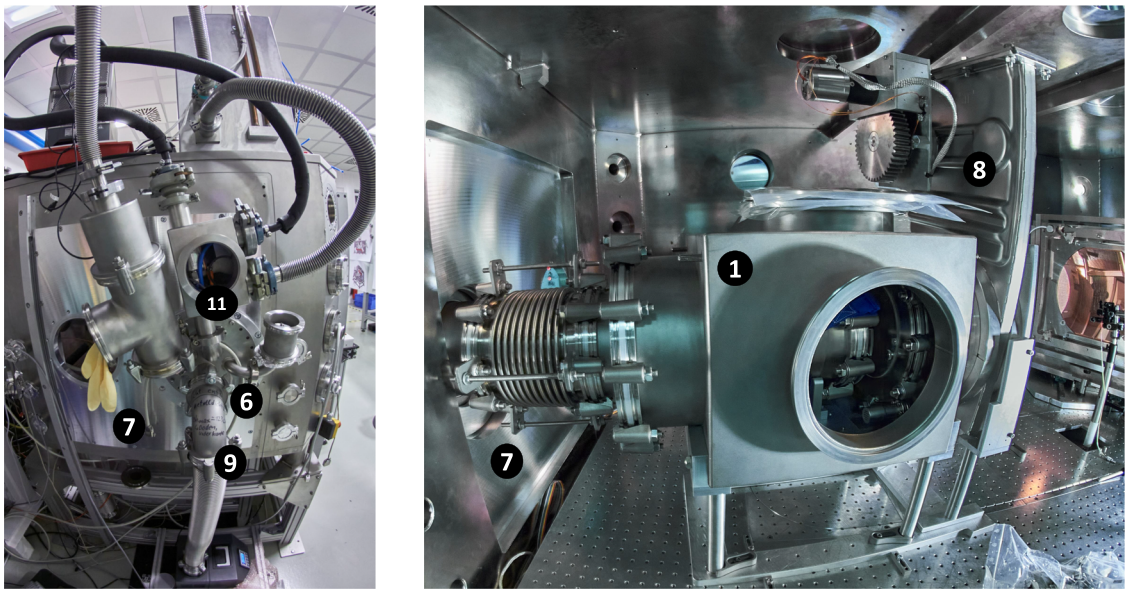

FIG. 2. Photograph of the target chamber during the setup phase at the PHELIX facility. The labels in the photos match the parts in Fig. 1. Left: Wiring outside of the chamber. All cables and instrumentation (e.g., a Pirani gauge) are covered by stainless steel vacuum components. This allows us to extend the Faraday cage to the EMP protective computer case, top right. The vacuum inside the EMP box is generated by the small turbo pumping station visible on the bottom. Right: Arrangement of the box inside the target chamber. Inside the outer Faraday cage ①, the inner Faraday cage for the JUNGFRAU detector and the beryllium window are visible. The backlighter is placed at the position of the optical post, visible on the right side.

the cut-off frequency for the ventilation holes is about 87 GHz. The frequency-dependent shielding effectiveness $SE_{dB}(f)$ of this array-like wave guide structure can be calculated via[11,12]

$$SE_{dB}(f) = 31.98\frac{l}{d}\sqrt{1-\left(\frac{f}{f_c}\right)^2} - 20\log(N), \quad (2)$$

with l being the length and N being the number of holes in the array. For our two beryllium window bypasses, the damping exceeds 200 dB up to a frequency of several tens of GHz. This is equivalent to a relative attenuation by a factor of 10^{10}. Since damping depends on the exact configuration of the electromagnetic field-structure, this value should be seen as a rough approximation.

III. IMPLEMENTATION AT THE PHELIX FACILITY

During the experiment at the PHELIX facility, pump-probe experiments with different types of targets were conducted. Standard radiography and grating-based phase-contrast imaging were applied as imaging techniques. The setup consists of four permanently placed components: A backlighter x-ray source, an object to be shocked, a deflecting magnet, and the detector. In the case of grating-based phase-contrast imaging, two additional gratings were placed in the beam path. The relevant parts of the experimental setup are introduced briefly.

A. Experimental setup

As an x-ray source, a laser pulse with a duration of 8 ps and an energy of about 30 J is shot at a 5 μm thin tungsten wire, creating a plasma that emits an x-ray flash with a broad energy spectrum.[5] During this process, electrons are ejected from the target. The resulting charge separation and compensating currents additionally generate an EMP.[6] According to Consoli *et al.*,[6] the magnitude of the EMP generated by the backlighter driver laser is about 20 kV/m at a distance of 1 m. The dominant x-ray energy for imaging with the PHELIX laser, a tungsten backlighter wire, and analog imaging plates was determined by Seifert *et al.*[13] and verified by Akstaller *et al.*[14] to be about 12 keV. As the JUNGFRAU detector has a similar energy-dependent sensitivity as the IP, the dominant x-ray energy for imaging is expected to be in the same range. Hence, the entire imaging setup was optimized for photons in an energy range between 10 and 12 keV.

A solid target, which is placed 30 mm away from the backlighter, is irradiated by a second laser pulse with 30 J of energy and a duration of a few ns to generate a plasma shock. Following[6] this, these laser-matter interactions also generate EMP pulses with amplitudes of about 2 kV/m at a distance of 1 m. A magnet designed to divert electrons and protons, preventing them from impinging on the detector, is placed downstream of the shock target.

The JUNGFRAU detector, enclosed by the EMP housing, is placed at a distance of 930 mm from the backlighter source. A view inside the target chamber with the EMP housing can be seen in Fig. 2, right side. The left image shows the wiring outside of the target chamber. To keep the Faraday shielding intact, all wires are guided by KF bellows, which are joined with clamping rings and aluminum seals.

B. Detector performance and imaging results

For each backlighter shot, 2500 individual images with an integration time of 500 μs each were taken. 500 of these were performed before the laser shot hit the target in order to clear out the pixel array and get the sensor closer to thermal equilibrium. Since the x-ray flash lasts only about 8 ps, it is well contained within a single acquisition. 2 s after the acquisitions are completed, detector pedestals are acquired. The pedestal is required to correct for the dark current in the silicon sensor.

During the experiment, the detector worked flawlessly, and not a single image was lost due to the EMP. One example image is shown in Fig. 3. It contains an attenuation image of a shocked foam target and was acquired without the grating setup. The dark vertical bar in the image is the target mount, which absorbs more photons than the surrounding material as it is fabricated from solid plastic. The greenish rectangular structure is a foam cylinder in which the shock propagates, viewed from the side. It shows higher pixel values due to less absorption compared to the solid plastics of the target mount. The foam is contained in a Kapton shell and has a thin aluminum coating on the side on which the laser is focused. In the image, the laser impinges on this backing from the right side through a small hole in the target mount, and the shock propagates toward the left edge of the foam.

The quality of the images obtained with this experimental setup is evaluated using the pixel values contained within the red rectangle shown in Fig. 3. The signal-to-noise ratio (SNR) is used, which is given by SNR = μ/σ, with μ being the mean and σ being the standard deviation of the intensity values measured in the different pixels. For the two images acquired without the grating setup, i.e., where an area without object structures is available, SNR values of about 103 and 74 are obtained, with one pixel covering a solid angle of 6.6×10^{-9} sr of the x-ray flux emitted from the source. To our knowledge, such a high SNR is not possible using imaging plates at the usual fluence of x-ray backlighters. A histogram of the intensity values within the red rectangle of both images can be found in the supplementary material of this publication (see Sec. V). The large difference in the SNR values probably stems from a significant difference in the deposited energy in the detector. One pixel in the image with the higher SNR acquired on average 44.5 MeV, while the image with the lower value only measured 35.3 MeV. This strong shot-to-shot fluctuation was

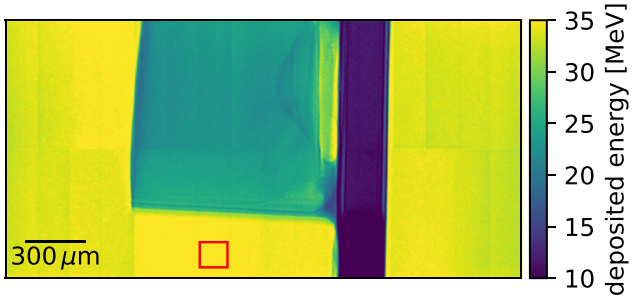

FIG. 3. Radiography of a PMMA foam (density 0.25 $\frac{g}{cm^3}$) that is exposed to a 1 ns laser pulse of 30 J from the right. The image is taken with an 8.5 ns delay after the laser pulse. The area denoted by the red rectangle is used to estimate the signal-to-noise ratio.

already observed in previous studies[14,15] and is inherent in x-ray backlighter sources.

C. EMP measurements

To validate the EMP protection of the detector housing, the EMP is measured at three different locations during the experiment. One Möbius antenna is placed between the outer and inner Faraday cages (Parts ① and ④ in Fig. 1). Another antenna is placed below the EMP box at roughly the same distance from the backlighter as the antenna inside box (900 mm). The third antenna is placed outside the target chamber, close to the connection between the EMP box and the outer wall (Part ⑥). A measurement in the inner Faraday cage/detector housing (Part ④) is not performed due to concerns that the antenna might also act as a sender if the EMP couples into the coaxial leads.

We used Möbius antennas with a diameter of 30 mm. Due to the symmetric output signal of these antennas (see Duncan)[16] a balanced-to-unbalanced transformer type TC-1-13MA+ from Mini-Circuits was used to match and add the signals. Multiple attenuators are used to reduce the induced voltage to a measurable and safe amplitude, depending on the position of the antenna. For additional protection, ultra-fast limiters are added. This signal is measured with a Tektronix MSO64B capable of measuring up to 8 GHz signals. Since every component is at least rated for 1 GHz and has a reasonably low damping for higher frequencies, the EMP-signal can be measured up to a frequency of about 4 GHz.

Figure 4 shows typical EMP signals generated by imaging a shocked foam target with a tungsten backlighter wire (the same setup as used to acquire Fig. 3). The left column contains the time evolution of the induced signal. The right side shows the frequency spectra of the pulses, calculated via a Fourier transform in a time interval of 1.0 μs starting at the time stamp of −0.2 μs. 0 μs marks the time when the laser hits the target. The voltages were rescaled with the applied attenuators. As only relative differences between the measurements are relevant for determining the damping of the shielding, the damping of the cables of equal length is omitted. Note that the y-scale varies by a few orders of magnitude between the antenna signals.

Comparing the signal inside the target chamber (blue curve) with the signal outside the target chamber (green curve), it can clearly be seen that the measured voltage amplitude is reduced by a factor of about 10. This has at least two reasons. First, the antenna outside the chamber is about twice the distance from the source. Second, the experimental chamber is constructed from stainless steel, and although it contains many feedthroughs and windows, it also

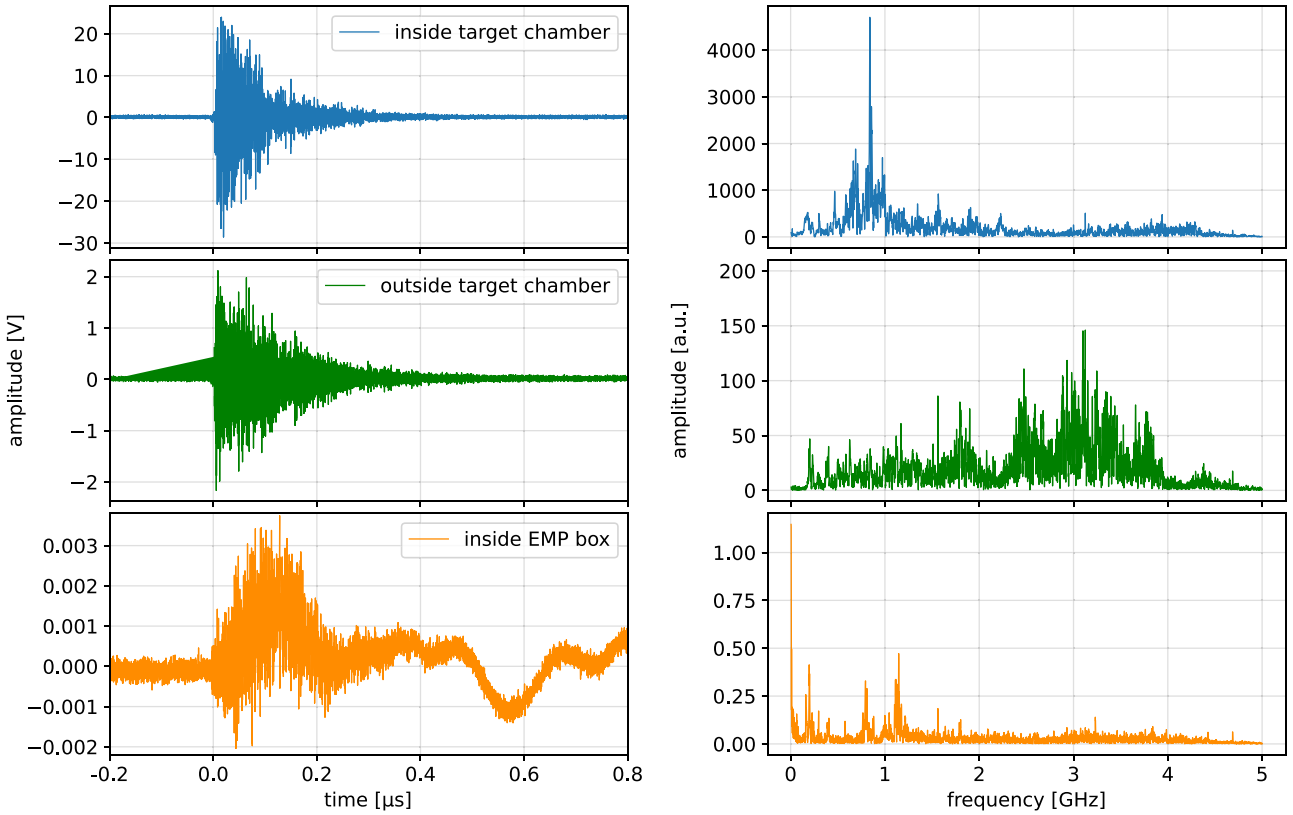

FIG. 4. Representative measurement of the EMP generated during pump-probe experiments at the PHELIX facility (30 J pulse energy each). Left: Time evolution of the induced voltage for three antennas placed in the PHELIX target chamber (top), outside the target chamber (middle), and inside the EMP box (bottom). Note the different scales of the vertical axes. Right: Frequency spectra of the signals shown on the left for the time range −0.2–0.8 μs.

acts as an incomplete Faraday cage. Furthermore, as can be seen in the right column of Fig. 4, the low frequencies are dampened significantly. Comparing the measurement inside the target chamber (blue curve) with the one inside the EMP box (orange curve) shows that the maximum measured amplitude is reduced by a factor of more than 6500. However, there is a prominent oscillation with a frequency of about 7.5 MHz inside the EMP box present, which persists even when the other frequency components of the EMP vanish at about 0.4 μs. To incorporate this circumstance, a frequency dependent analysis is performed. This is performed by defining a field-strength ratio FSR, which is calculated using

$$\mathrm{FSR} = \frac{S_{\mathrm{chamber}}}{S_{\mathrm{box}}}, \tag{3}$$

with S_{box} and S_{chamber} being the amplitudes of the frequency components inside and outside the EMP box. In the upper plot of Fig. 5, the frequency spectra inside the target chamber (blue curve) and inside the EMP box (orange curve) are plotted on a semi-log scale. Except for low frequencies, the difference in amplitude is nearly constant. This can also be observed in the field strength ratio, shown in the lower plot of Fig. 5, calculated with Eq. (3). The FSR is about 100 in the low frequency range and exceeds 1000 at ~100 MHz. At about 700 and 900 MHz, when the frequency spectrum of the measured EMP signal inside the target chamber has a peak, the FSR increases in parts up to 10 000. For frequencies higher than 1 GHz, the field-strength ratio is on average higher than 1000. The fact that an EMP signal is still measured within the outer Faraday cage indicates a leak. One conceivable EMP point of ingress through the outer Faraday cage is the turbomolecular pumping station (see left image in Fig. 2) since it is the only part that is not designed as a perfect Faraday cage.

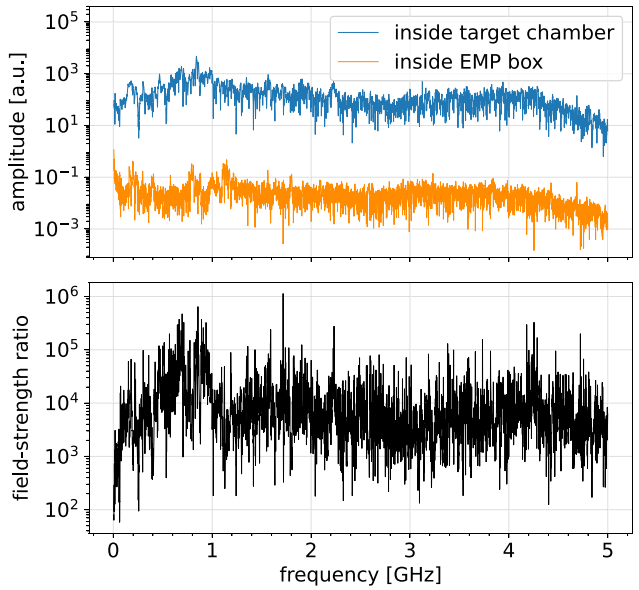

FIG. 5. Top: Semi-log plot of the frequency spectra inside the target chamber (blue) and inside the EMP box (orange). Bottom: Field-strength ratio of the EMP box over the whole displayed frequency range calculated with Eq. (3).

However, as the measurement is performed between the two Faraday cages, it is probable that the EMP is even lower inside the innermost cage, meaning that the presented setup has even higher EMP protection. For a better grading of the measured signals and their associated EMP, it is worth mentioning that outside the target chamber, digital detectors and devices could be operated without any protection. Hence, it is reasonable to assume that the presented housing will also protect the detector in experiments with way higher laser-pulse energies and, thus, stronger EMPs.

IV. CONCLUSION AND OUTLOOK

A highly effective and x-ray transparent EMP shielding for digital x-ray detectors is presented. During a high-energy pump-probe experiment, the EMP-shielding successfully protected the JUNGFRAU detector, placed inside the target chamber of the PHELIX high power laser facility (GSI Helmholtzzentrum für Schwerionenforschung GmbH).

Beryllium was chosen as an x-ray entrance window as it is low-absorbing and electrically conductive. This keeps the protective Faraday cage for the detector as close to perfect as possible. The relative damping of the EMP, defined as the field-strength ratio of two probes, was measured with two antennas to be in the order of 1000 for frequencies higher than 100 MHz and about 100 for lower frequencies. This assured interruption-free operation of the detector for two weeks without any loss of image data. Furthermore, the EMP box serves as its own vacuum box, making it possible to cool down the detector to temperatures below 0 °C independent of the experimental chamber's pressure without any issue of condensation or impact on evacuation time. This makes it possible to stabilize the detector temperature to a fraction of a Kelvin, enabling perfect conditions for the detector's dark-current correction while retaining high experimental repetition rates.

With the possibility of using a low-noise direct-detecting x-ray detector like the JUNGFRAU, the achievable image quality at x-ray backlighters will significantly improve compared to other detectors or analog imaging plates.[17] Signal-to-noise ratio values exceeding 100 were obtained in the free-field with the presented setup. Theoretically, the obtained image quality is only limited by the noise stemming from the x-ray source.[9] Adapting the concept introduced in this paper also allows using other types of digital detectors and devices in experiments with a strong EMP present, enabling novel diagnostics.

SUPPLEMENTARY MATERIAL

Two documents are provided as supplementary material. The first document is an interactive 3D-PDF, which contains the CAD model of the EMP-box. To view the model, a suitable PDF-viewer (e.g., Adobe Acrobat Reader) must be used and the document's content trusted. In the *Model Tree*, all individual parts can be selected or hidden.

In the second document, the data used for determining the SNR of the detector images are presented in more detail. Both detector images are depicted, and zoom-in plots of the red-framed area are shown. In addition to that, histograms of the pixels' intensity values are given.

ACKNOWLEDGMENTS

The results presented here are based on the experiment P-21-00013, which was performed at the PHELIX facility at the GSI Helmholtzzentrum für Schwerionenforschung, Darmstadt (Germany), in the frame of FAIR Phase-0. We would like to give special thanks to the PHELIX operation team. Furthermore, we would like to acknowledge Robbie Wilson and his team (University of Strathclyde, Glasgow) for providing the opportunity to participate in their beamtime at the PHELIX laser, where we tested the first version of the EMP housing. Additionally, we would like to acknowledge the whole team of the mechanical workshop for manufacturing our experimental setup and Hennry Schott and Thorsten Kühn for their support and ideas (all ECAP). Daniel Kübrich for his suggestions and thoughts regarding the prototype of the EMP housing (Friedrich-Alexander University). This work was funded by the Deutsche Forschungsgemeinschaft (DFG) under Grant No. 452935060. The work of A. S. Martynenko was supported by the Alexander von Humboldt Foundation.

AUTHOR DECLARATIONS

Conflict of Interest

The authors have no conflicts to disclose.

Author Contributions

Stephan Schreiner and **Constantin Rauch** contributed equally to this work.

Stephan Schreiner: Conceptualization (lead); Data curation (lead); Formal analysis (lead); Investigation (lead); Methodology (lead); Project administration (lead); Resources (equal); Software (supporting); Validation (lead); Visualization (lead); Writing – original draft (lead); Writing – review & editing (lead). **Constantin Rauch**: Conceptualization (lead); Data curation (lead); Formal analysis (lead); Investigation (lead); Methodology (lead); Resources (equal); Software (lead); Validation (equal); Visualization (lead); Writing – original draft (lead); Writing – review & editing (lead). **Bernhard Akstaller**: Conceptualization (supporting); Data curation (supporting); Resources (supporting); Software (equal); Writing – review & editing (supporting). **Paulina Bleuel**: Data curation (supporting); Formal analysis (equal); Investigation (equal); Methodology (supporting); Software (equal); Validation (equal); Visualization (supporting); Writing – review & editing (supporting). **Eric Fröjdh**: Data curation (supporting); Resources (equal); Software (equal); Supervision (supporting); Writing – review & editing (supporting). **Artem S. Martynenko**: Conceptualization (equal); Data curation (supporting); Resources (supporting); Writing – review & editing (supporting). **Aldo Mozzanica**: Data curation (equal); Resources (equal); Software (supporting); Supervision (supporting); Writing – review & editing (supporting). **Paul Neumayer**: Conceptualization (equal); Data curation (supporting); Project administration (supporting); Resources (supporting); Writing – review & editing (supporting). **Leonard Wegert**: Conceptualization (equal); Data curation (equal); Resources (equal); Writing – review & editing (supporting). **Bernhard Zielbauer**: Conceptualization (equal); Data curation (equal); Project administration (equal); Supervision (supporting); Writing – review & editing (supporting). **Adrian Zink**: Data curation (supporting); Methodology (supporting); Resources (supporting); Writing – review & editing (supporting). **Gisela Anton**: Conceptualization (supporting); Formal analysis (supporting); Funding acquisition (equal); Investigation (supporting); Supervision (equal); Writing – review & editing (supporting). **Thilo Michel**: Conceptualization (supporting); Funding acquisition (equal); Investigation (supporting); Supervision (equal); Writing – review & editing (supporting). **Stefan Funk**: Conceptualization (supporting); Funding acquisition (lead); Investigation (supporting); Project administration (supporting); Resources (equal); Supervision (equal); Writing – review & editing (supporting).

DATA AVAILABILITY

The data that support the findings of this study are available within the article and its supplementary material and from the corresponding author upon reasonable request.

REFERENCES

[1] S. Le Pape, L. F. Berzak Hopkins, L. Divol, A. Pak, E. L. Dewald, S. Bhandarkar, L. R. Bennedetti, T. Bunn, J. Biener, J. Crippen *et al.*, "Fusion energy output greater than the kinetic energy of an imploding shell at the National Ignition Facility," Phys. Rev. Lett. **120**, 245003 (2018).

[2] J. F. Hansen, H. F. Robey, R. I. Klein, and A. R. Miles, "Experiment on the mass stripping of an interstellar cloud following shock passage," Astrophys. J. **662**, 379 (2007).

[3] R. I. Klein, K. S. Budil, T. S. Perry, and D. R. Bach, "The interaction of supernova remnants with interstellar clouds: Experiments on the Nova laser," Astrophys. J. **583**, 245 (2003).

[4] H. F. Robey, T. S. Perry, R. I. Klein, J. O. Kane, J. A. Greenough, and T. R. Boehly, "Experimental investigation of the three-dimensional interaction of a strong shock with a spherical density inhomogeneity," Phys. Rev. Lett. **89**, 085001 (2002).

[5] B. Borm, D. Khaghani, and P. Neumayer, "Properties of laser-driven hard x-ray sources over a wide range of laser intensities," Phys. Plasmas **26**, 023109 (2019).

[6] F. Consoli, V. T. Tikhonchuk, M. Bardon, P. Bradford, D. C. Carroll, J. Cikhardt, M. Cipriani, R. J. Clarke, T. E. Cowan, C. N. Danson *et al.*, "Laser produced electromagnetic pulses: Generation, detection and mitigation," High Power Laser Sci. Eng. **8**, E22 (2020).

[7] D. Kocon, D. Klir, J. Krasa, T. Lastovicka, L. Pribyl, R. Vrana, E. Beamlines, C. Granja, J. Jakubek, and M. Platkevic, "Operating semiconducFrtor Timepix detector with optical readout in an extremely hostile environment of laser plasma acceleration experiment," in *2nd International Beam Instrumentation Conference (IBIC 2013)*, p. 208.

[8] A. Mozzanica, M. Andrä, R. Barten, A. Bergamaschi, S. Chiriotti, M. Brückner, R. Dinapoli, E. Fröjdh, D. Greiffenberg, F. Leonarski *et al.*, "The JUNGFRAU detector for applications at synchrotron light sources and XFELs," Synchrotron Radiat. News **31**, 16–20 (2018).

[9] A. Mozzanica, A. Bergamaschi, M. Brueckner, S. Cartier, R. Dinapoli, D. Greiffenberg, J. Jungmann-Smith, D. Maliakal, D. Mezza, M. Ramilli *et al.*, "Characterization results of the JUNGFRAU full scale readout ASIC," J. Instrum. **11**, C02047 (2016).

[10] B. Henke, E. Gullikson, and J. Davis, "X-ray interactions: Photoabsorption, scattering, transmission, and reflection at $E = 50–30\,000$ eV, $Z = 1–92$," At. Data Nucl. Data Tables **54**, 181 (1993).

[11] S. Yoon, K. Jeong, S. Mumtaz, and E. H. Choi, "Electromagnetic pulse shielding effectiveness of circular multi-waveguides for fluids," Results Phys. **16**, 102946 (2020).

[12] W. Bereuter and D. Chang, "Shielding effectiveness of metallic honeycombs," IEEE Trans. Electromagn. Compat. **EMC-24**, 58–61 (1982).

[13]M. Seifert, M. Weule, S. Cipiccia, S. Flenner, J. Hagemann, V. Ludwig, T. Michel, P. Neumayer, M. Schuster, A. Wolf, G. Anton, S. Funk, and B. Akstaller, "Evaluation of the weighted mean X-ray energy for an imaging system via propagation-based phase-contrast imaging," J. Imaging **6**, 63 (2020).
[14]B. Akstaller, S. Schreiner, F. Hofmann, P. Meyer, P. Neumayer, M. Schuster, A. Wolf, B. Zielbauer, V. Ludwig, T. Michel, G. Anton, and S. Funk, "Single-shot grating-based phase-contrast imaging of a micrometer sample at a laser-driven x-ray backlighter source," J. Instrum. **16**, P06021 (2021).
[15]S. Schreiner, B. Akstaller, L. Dietrich, P. Meyer, P. Neumayer, M. Schuster, A. Wolf, B. Zielbauer, V. Ludwig, T. Michel, G. Anton, and S. Funk, "Noise reduction for single-shot grating-based phase-contrast imaging at an X-ray backlighter," J. Imaging **7**, 178 (2021).
[16]P. Duncan, "Analysis of the Moebius loop magnetic field sensor," IEEE Trans. Electromagn. Compat. **EMC-16**, 83–89 (1974).
[17]M. Bech, O. Bunk, C. David, P. Kraft, C. Brönnimann, E. F. Eikenberry, and F. Pfeiffer, "X-ray imaging with the PILATUS 100k detector," Appl. Radiat. Isot. **66**, 474–478 (2008).